



HAL
open science

Influence of material properties and boundary conditions on patient-specific models.

Bastien Goin, Jean-Baptiste Renault, Lisa Thibes, Patrick Chabrand

► **To cite this version:**

Bastien Goin, Jean-Baptiste Renault, Lisa Thibes, Patrick Chabrand. Influence of material properties and boundary conditions on patient-specific models.. *Computer Methods in Biomechanics and Biomedical Engineering*, 2021, 24 (4), pp.429–439. 10.1080/10255842.2020.1833326 . hal-03553383

HAL Id: hal-03553383

<https://hal.science/hal-03553383v1>

Submitted on 15 Apr 2022

HAL is a multi-disciplinary open access archive for the deposit and dissemination of scientific research documents, whether they are published or not. The documents may come from teaching and research institutions in France or abroad, or from public or private research centers.

L'archive ouverte pluridisciplinaire **HAL**, est destinée au dépôt et à la diffusion de documents scientifiques de niveau recherche, publiés ou non, émanant des établissements d'enseignement et de recherche français ou étrangers, des laboratoires publics ou privés.

Influence of material properties and boundary conditions on patient-specific models

Bastien Goin , Jean-Baptiste Renault , Lisa Thibes & Patrick Chabrand

Influence of material properties and boundary conditions on patient-specific models

Bastien Goin^a, Jean-Baptiste Renault^{a,b†}, Lisa Thibes^a and Patrick Chabrand^{a,b}

^aCNRS, ISM, Aix-Marseille Université, Marseille, France; ^bDepartment of orthopaedics and Traumatology, APHM, Institute for Locomotion, Sainte-Marguerite Hospital, Marseille, France

ABSTRACT

Patient-specific finite element models (PSFEM) are becoming more and more used. Different methods for assigning their material properties were studied on PSFEMs of 9 tibias along with the minimal required length of the CT acquisition window. Material properties are generally attributed to the PSFEM using relationships linking the grayscale of CT scans to the elasticity moduli. Using cortical-specific and trabecular-specific relationships or a generic one, did not result in significant differences. However, the use of homogeneous elastic moduli in the cortical and trabecular regions led to considerable differences. The result highlight that the PSFEM must comprise at least 40% of the tibia to ensure consistent results in the proximal 20%.

Introduction

Osteoarthritis is a multi-factorial degenerative joint disease involving the destruction of the cartilage, thus resulting in pain and functional discomfort (Arden and Nevitt 2006). Arthritis of the knee has a prevalence in males that increases from 2.1% at 40 years old to 10.1% at 75, and in females from 1.6% to 14.9% respectively (Guillemin et al. 2011). When most of the joint surface is damaged and is limiting the patient's functional ability, total knee arthroplasty (TKA) is considered. In the USA, TKA is estimated to have been performed on 1.52% of the overall population in 2010 (Maradit Kremers et al. 2015), while 60 355 revision surgeries were performed between October 2005 and December 2006 (Bozic et al. 2010). Nine causes of TKA failure leading to surgical revision have been identified, including bone tissue resorption at the interface between the bone and the implant, and peri-prosthetic fracture, respectively responsible for 3.2% and 1.5% of surgical revision. These causes are often associated with poor stress distribution and can, therefore lead to peri-prosthetic bone resorption, also known as stress shielding, and periprosthetic pain (Wolff 1893; Completo et al. 2009). Persistent pain and functional discomfort leave one out of five TKA patients dissatisfied (Bourne

et al. 2010). To explain these phenomena, numerical simulations based on finite element analysis (FEA) have been performed over the last four decades (Taylor and Prendergast 2015). Generally, such studies make simplifying assumptions to enable calculation. Some of these hypotheses base both the choice of material properties and the boundary conditions on clinical literature, but without considering the patient's specific features (Table 1) (Castro et al. 2015; Brihault et al. 2016; El-Zayat et al. 2016; Innocenti et al. 2016; Thompson et al. 2016; Baliga et al. 2018).

Technological advances in additive manufacturing enable the design of implants specific to the patients, both geometrically and mechanically (He et al. 2018). However, preoperative planning must be provided for in the methodology. Also known as the virtual operating theater, this is aimed at helping surgeons adapt their approach to the specific features of each patient (Munier et al. 2017). 3D reconstructions of anatomical parts obtained with CT scan segmentation allow to account for patient-specific geometry (El-Zayat et al. 2016; Thompson et al. 2016). Several methodologies/strategies to assign patient specific mechanical properties to PSFEM from quantitative CT-scan coexists. PSFEM classically derive heterogenous material properties from the HU field obtained with quantitative CT-scan (Helgason et al. 2008; Knowles et al. 2016) and

Table 1. Synthesis of different methods of assignment of material properties and boundary conditions from the recent scientific literature in the field of FEM studies of knee prostheses.

Authors	FE Model Geometry	Material properties	Fully constrained region	Muscles and ligaments	Loading case
Baliga et al. 2018	Patient-specific	$\rho = 1.037 \times 10^{-4}(HU + 1000)$ for $HU \leq 138$ $\rho = 1.037 \times 10^{-4}(HU + 1000)$ for $HU > 138$ $E = 2003\rho^{1.56}$ (in MPa) for $\rho \leq 0.778$ $E = 2875\rho^{3.0}$ (in MPa) for $\rho > 0.778$ Poisson's ratio : $\nu = 0.30$	/	/	Three kinds of maximal axial compression loading (3360, 4108 et 4261 Newton) during walking medial (55%) and lateral (45%)surfaces of the polyethylene support.
Brihault et al. 2015	SawBones	Material Cortical bone E_1 (MPa) 11 500 E_2 (MPa) 11 500 E_3 (MPa) 17 000 ν_{12} 0,51 ν_{13} 0,31 ν_{23} 0,31 Cancellous bone E (MPa) 2130 ν 0,3 Cancellous bone: $E = 104 \text{ MPa}$, $\nu = 0.30$ Compact bone: $E = 16,700 \text{ MPa}$, $\nu = 0.30$	Osteoporotic / Osteopenic / Physiological /	/	A constant axial compression (200 N) on the femoral head where applied during the motricity task.
Castro et al. 2014	SawBones	Cancellous bone: $E = 104 \text{ MPa}$, $\nu = 0.30$ Compact bone: $E = 16,700 \text{ MPa}$, $\nu = 0.30$	Proximal extremity of femur	/	Three cases of axial compression: Climbing stairs = 2963 N Descending stairs = 2668 N Isometric exercise = 2698 N evenly distributed (50 : 50) between medial and lateral condyles.
El-Zayat et al. 2016	SawBones	Cortical bone Transversally isotropic Cancellous bone Isotropic	Distal part of tibia	Patellar tendon producing 3518 N in total	A constant axial compression (200 N) on the femoral head where applied during the motricity task.
Innocenti et al. 2016	Patient-specific	Cortical bone Transversally isotropic Cancellous bone Isotropic	Distal part of tibia	Collateral and cruciate ligaments; mechanical behavior supposed to be linearly elastic isotropic.	A vertical load of 2000 N reproducing the maximum axial force of the knee during walking.
Thompson et al. 2015	Patient-specific	$\Omega_{\text{physiological tibia}} = 700 \text{ MPa}$ $\Omega_{\text{Tibia metabolic pathology}} = 350 \text{ MPa}$	/	/	A vertical load of 2100 N reproducing the maximum axial force of the knee during walking evenly distributed (50:50) between the medial and lateral condyles.

Table 2. Method of assignment of material properties specific to each of the 3 models tested (DHoM, nDHeM and DHeM). "X" represents T10 elements, "E" the Young's modulus expressed in MPa, "ρ" the apparent bone density expressed in Kg/m³ and "ν" the Poisson's ratio denoted without units.

Models / Conditions	PSFEM Tibia		
	Ω_{Cort}	Ω_{Trab}	Ω_{Tibia}
(DHoM) Differentiated Homogeneous Model	$E(X) = 20\,000\text{ MPa}$	$E(X) = 800\text{ MPa}$	$\nu(X) = 0.3$
References	(Williams and Lewis 1982; Keaveny and Hayes 1993)		
(nDHeM) non-Differentiated Heterogeneous Model		$E(X) = 0,916\text{ Hu}(X) + 114$ $E(X) = 0,51\ \rho(X)^{1,37}$	$\nu(X) = 0.3$
$E = f(\text{Hu})$			
(DHeM) Differentiated Heterogeneous Model	$E(X) = 13\ \rho(X) - 3842$ $\rho(X) = \text{Hu}(X)$	$E(X) = 0,51\ \rho(X)^{1,37}$ $\rho(X) = 0,916\text{ Hu}(X) + 114$	$\nu(X) = 0.3$
References		(Rho et al. 1995)	

assign them in differentiated (Baliga et al. 2018) or non-differentiated fashion to the trabecular and bone regions (Taddei et al. 2006a), while generic models assign homogenous material properties in different subregion of the bones (Au et al. 2005; Innocenti et al. 2016), It would, therefore, be of great interest to evaluate the differences, in terms of biomechanical fields, resulting from the use of different material properties assignment strategies and integrates into this process, along with geometrical criteria, patient-specific mechanical properties via empirical formulae linking the mechanical properties of the tibia to the CT scan acquisitions (Helgason et al. 2008; Knowles et al. 2016). Moreover, the acquisition-window height of the CT scans required for a patient-specific finite element model (PSFEM) could be minimized to reduce patients radiation exposure (Brenner and Hall 2007), acquisition time and PSFEM size. In the virtual operating theater methodology, the acquisition window height should be reduced without altering the variables of interest in the volume of interest (VOI).

As far as we know, the bias due to differences in the location of the fully constrained face of PSFEM has never previously been investigated (Table 1). It has, however, been observed that any coarse approximation of material properties or boundary conditions in the FEA can dramatically distort the results of simulations (Mesfar and Shirazi-Adl 2006; Taddei et al. 2006b; Heyland et al. 2015). Yet there is no consensus on choice either of material properties or of boundary conditions. Here, we sought to quantify: (i) the difference, in terms of classic biomechanics output fields, between the different material modelling strategies of PSFEM of the human tibia; (ii) the minimum height required for the CT scan acquisition window to ensure consistent results in our VOI.

Materials and methods

Data acquisition

Nine datasets were collected with images in the DICOM format hosted on the SICAS Medical Image Repository and provided by the SMIR team (Kistler et al. 2013). Each dataset contains a post-mortem full-body CT scan acquisition (Siemens Somatom Emotion 6, 130 KVp, 125 mAs, $0.9512 \times 0.9512 \times 0.6\text{ mm}^3$ voxel size). The corresponding acquisition method used a normalized, reproducible protocol aimed at limiting potential biases. The human subjects were selected as representative of the population; thus, our sampled population consisted of 6 men and 3 women aged between 22 and 90 years old (mean: 64.2). Only the left tibia was considered in this study.

Geometry

Segmentations of the 9 left tibias from the CT acquisition were performed with Mimics 17.0 (Materialize, Louvain, Belgium). Segmentation methods consisted of first, automated global thresholding of the image stacks (van Eijnatten et al. 2018), followed by manual refinements to improve the fidelity of the 3D reconstruction of each tibia. Secondly, a cortical bone mask was obtained by merging the 2-voxel-thick external layer of the initial mask with the mask of voxels with HU values over 600. The trabecular mask resulted from the boolean subtraction of the cortical mask from the global mask of the tibia.

Mesh generation

Each of the 9 tibias was volumetrically meshed using the GMSH software with a Python script. The prescribed element sizes were identical for all subjects. Second-order tetrahedral elements (T10) were chosen to mesh the non-regular geometry of our models

Table 3. Synthesis of forces and their orientations applied to each of our 9 PSFEMs with: contralateral heel strike (CTL_HS), contralateral toe off (CTL_TO), getting up from a chair (CU). Orientation of the forces are defined relatively to the upward tibia mechanical axis by: α - the angle between mechanical axis and the force when projected on the sagittal plane, it is positive for anteriorly oriented forces; β - the angle between the mechanical axis and the force when projected on the frontal plane, it is positive for medially oriented forces. "-" denote negligible muscle force. Adapted from Kuster et al. 1997, Wimby et al. 2009 and Sasaki and Neptune 2010.

Load Cases	Knee Flexion	Medial Femoral Force			Lateral Femoral Force			Patellar Tendon			Semimembranosus			Biceps Femoris			Semitendinosus		
		Force (N)	β (°)	α (°)	Force (N)	β (°)	α (°)	Force (N)	β (°)	α (°)	Force (N)	β (°)	α (°)	Force (N)	β (°)	α (°)	Force (N)	β (°)	α (°)
CTL_TO	15°	1750	0	-180	770	0	-180	560	9	14	170	-7	-16,1	85	11,8	-9,6	70	7,1	18,7
CTL_HS	5°	1120	0	-180	630	0	-180	550	11	16	-	-	-	65	4,9	-7,9	-	-	-
CU	90°	1800	0	-180	1000	0	-180	2500	1	-4	-	-	-	-	-	-	-	-	-

(Viceconti et al. 1998), and a convergence test of the mesh was performed. Each element had a mean edge length of approximately 2.5 mm, and each model was composed of approximately 110 000 elements yielding a total of 550 000 degrees of freedom (Polgar et al. 2001). A single mesh was generated for each PSFEM, allowing element-wise comparison between the simulation results of the conditions investigated.

Material properties

Three different material assignment methods were compared (Table 2): (i) the cortical/trabecular differentiated homogeneous models (DHoM), where the Young's modulus is fixed at one constant value in the cortical subvolume of the tibia and at another constant value in the trabecular subvolume; (ii) the differentiated heterogeneous model (DHeM), where two different mathematical relationships between the HU and the Young's modulus are respectively used for the trabecular and cortical subvolumes of the tibia; (iii) the non-differentiated heterogeneous model (nDHeM), where a single mathematical relationship is used for the whole tibia volume. The Young's moduli were uniform within each element and computed as the average of Young's moduli directly derived from each voxel Hounsfield Unit intersecting the element (Taddei et al. 2007). Bone materials were assumed to be isotropic and to present linear elastic properties for all 3 studied conditions, DHoM, nDHeM, and DHeM (Table 2). Twenty-seven models were obtained, 3 for each condition applied to the 9 PSFEMs. For each T10 meshing element of the two heterogeneous conditions, previously published relations between bone density and gray level in the CT scan acquisitions were used (Knowles et al. 2016). These relations were then linked to empirical mathematical models to compute the Young's modulus of each element (Helgason et al. 2008).

Boundary conditions

Assignment of reference points

Three points were manually placed on each of the 9 PSFEMs, using 3-Matic software (Materialize, Louvain, Belgium). They were positioned at the center of the medial and lateral condyles, and at the center of the articular surface of the ankle. This setup allowed us to determine the length of the tibia for all individuals and then automatically fully constrained (fixed nodes) several selections of nodes more distal to

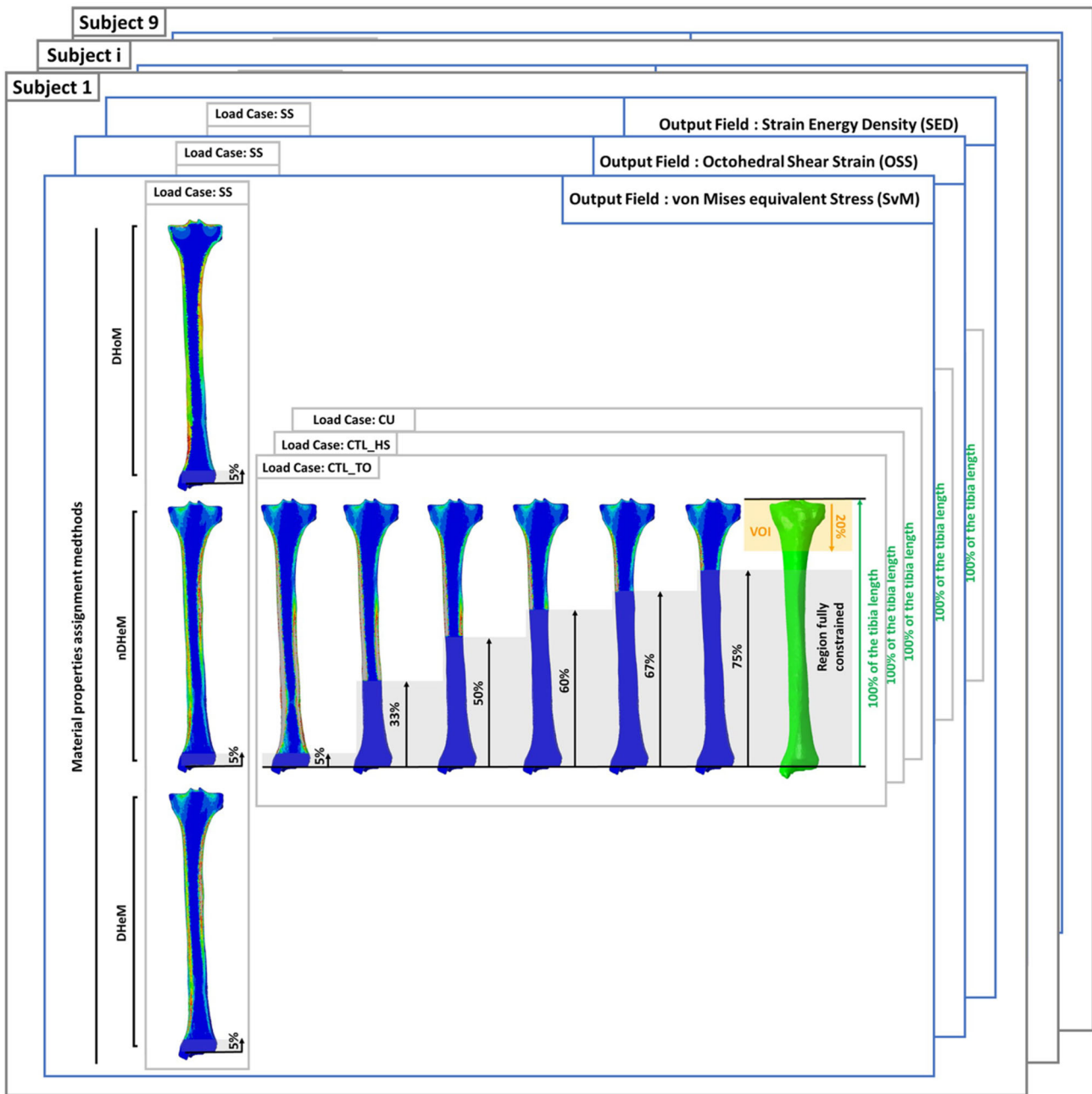


Figure 1. Schematic of the method use to obtain the results for the different levels of the fully-constrained region and the different strategy used to assign the material properties. The method was identical for each of the 9 subjects.

those at the level of interest, using a Python script on the Abaqus software.

Loading and muscle forces

The centers of the three regions, where the principal muscle forces were applied were determined for each PSFEM by referencing to an anatomy book and correspond to the patellar ligament of the knee and main muscle groups described in Table 3. These muscles were the only ones considered in our PSFEM because of their significant influence on the knee joint under

the simulated conditions (DeFrate et al. 2007; Adouni et al. 2012). The femoral contact forces were cubically distributed on disks centered on the medial and lateral reference points of the tibial condyles. The impact of material assignment methods was assessed on a single load case. A 2000 N femoral force (collinear with tibia mechanical axis) was applied to the tibia, with 800 N on the lateral reference point and 1200 N on the medial reference point (Taylor et al. 2004). The impact of constrained level was assessed by applying forces for 3 simulated load cases: 1)

Table 4. Slope (a) and linear regression determination (R²) of inter-model comparisons (DHoM, nDHeM and DHeM), according to the 3 variables OSS, ESEDEN (SED) and SvM of the 9 PSFEMs.

PSFEM	Octahedral shear strain						Strain energy density (mm ³)						Von Mises stress (MPa)					
	DHoM vs. nDHeM		DHoM vs. DHeM		nDHeM vs. DHeM		DHoM vs. nDHeM		DHoM vs. DHeM		nDHeM vs. DHeM		DHoM vs. nDHeM		DHoM vs. DHeM		nDHeM vs. DHeM	
	a	R ²	a	R ²	a	R ²	a	R ²	a	R ²	a	R ²	a	R ²	a	R ²	a	R ²
8	0.734	0.588	0.744	0.647	0.953	0.973	1.379	0.723	1.179	0.731	0.843	0.984	0.613	0.601	0.639	0.589	1.048	0.991
30	1.020	0.539	1.020	0.604	0.927	0.961	1.809	0.810	1.538	0.776	0.862	0.985	0.590	0.634	0.614	0.614	1.047	0.984
38	1.663	0.454	1.661	0.581	0.848	0.923	4.634	0.721	3.537	0.731	0.751	0.981	0.879	0.564	0.877	0.584	0.968	0.974
92	0.365	0.369	0.375	0.461	0.903	0.965	0.843	0.571	0.735	0.618	0.834	0.991	0.646	0.711	0.691	0.714	1.064	0.994
168	0.912	0.529	0.920	0.582	0.952	0.977	1.644	0.684	1.405	0.654	0.865	0.980	0.594	0.600	0.605	0.556	1.049	0.983
170	0.638	0.480	0.644	0.550	0.925	0.964	1.431	0.788	1.197	0.788	0.832	0.988	0.619	0.630	0.659	0.635	1.056	0.993
417	0.878	0.439	0.882	0.512	0.916	0.969	1.581	0.553	1.368	0.563	0.849	0.980	0.521	0.455	0.550	0.458	1.042	0.982
522	0.868	0.534	0.873	0.605	0.947	0.969	1.539	0.724	1.297	0.728	0.833	0.983	0.636	0.619	0.665	0.617	1.043	0.992
547	0.757	0.483	0.769	0.546	0.942	0.972	1.662	0.734	1.384	0.696	0.846	0.981	0.586	0.573	0.599	0.537	1.048	0.986
Mean	0.871	0.493	0.877	0.565	0.934	0.964	1.836	0.701	1.515	0.698	0.835	0.984	0.632	0.599	0.655	0.589	1.041	0.987
SD	0.493	0.067	0.349	0.055	0.033	0.016	1.084	0.087	0.698	0.074	0.034	0.004	0.100	0.069	0.093	0.071	0.028	0.006

contralateral toe-off (CTL_TO) of the gait cycle, 2) contralateral heel-strike (CTL_HS) of the gait cycle, 3) peak force while getting up from a chair (CU). Details of the forces are given in Table 3.

Level of the fully-constrained distal face

Using the reference points, we defined, via a Python script, 6 different positions for the fully-constrained distal face of the PSFEM (5%, 33%, 50%, 60%, 67% and 75% of the full length of the tibia). Every node located distal to the constrained level was fully constrained (fixed). The 5% level was chosen as the control condition, corresponding to the most representative physiological condition of the articulation of the ankle. Each VOI corresponded to the proximal 20% of the associated tibia (see Figure 1).

Finite element analysis

FEA was performed with Abaqus/Standard 6.14-2 (Dassault Systems, Vélizy-Villacoublay, France). The output data were (i) octahedral shear strain (OSS) corresponding to the overall distortion of all the integration points inside each T10 element (Stadelmann et al. 2009); (ii) strain energy density (SED), in mJ per mm³, standing for accumulated energy during the PSFEM loading (Taddei et al. 2006b); (iii) von Mises stress (SvM), in MPa, computed at the four integration points of T10 elements. The sensitivity of the output data within the VOIs could be quantified for all PSFEMs involving the same static loading and depending on both the level of constraint and the material properties assignment methods.

Statistical analysis

Three mechanical properties were investigated using R-Studio: OSS, SED, and SvM. The statistical difference between the results for each studied condition, DHoM, nDHeM, and DHeM, was verified by applying a Friedman test between two separate datasets. The significance level was set at $p < 0.01$. The test also gives the R² coefficient of determination between the values at the identical integration points of the two tested conditions. Finally, the slopes of the linear regressions were computed.

Results

Modelling of material properties

The correlation between PSFEM datasets was investigated through the coefficient of determination R²

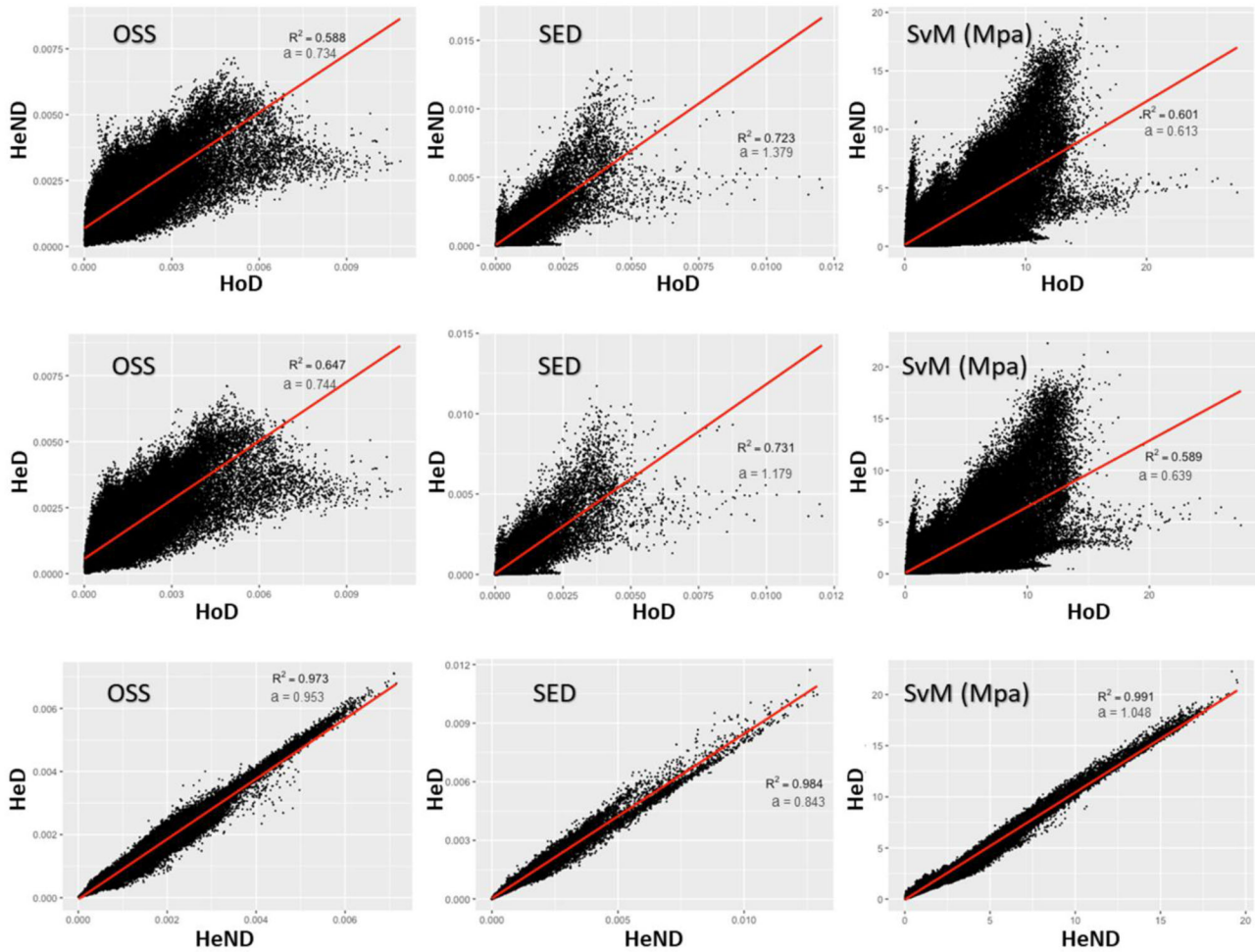


Figure 2. Example of results when investigating the impact of material assignment strategy. The plots here present element-wise linear regression of FEA results for the different methods of assigning material properties to the PSFEMs.

according to the three variables OSS, SED and SvM, with results shown in Table 4. The statistical Friedman tests yielded significant results ($p < 0.001$). The R^2 coefficient was roughly equal to 0.98 when nDHeM to DHeM conditions were compared, for all variables in all PSFEMs (Figure 2). Comparing the mean R^2 coefficients of conditions DHoM vs. nDHeM and DHoM vs. DHeM according to the three variables (OSS, SED, and SvM) weakly explains the variances found (Figure 2).

Constrained region level

To explain the variance in constraint levels (from 33% to 75%), the correlation between the PSFEM datasets was investigated through the coefficient of determination R^2 according to the three variables (OSS, SED and SvM). Results are shown in Table 5. Pearson correlation tests yielded significant results ($p < 0.0001$). Both the mean absolute differences and

the slope coefficients of the linear regression lines were computed relative to the 5% base case. For all conditions and variables in this study, we obtained $a = 1$ and $R^2 = 1$ for levels of constraint located at 33%, 50%, and 60% of the tibia length. Consequently, there were no variations for levels of integration ranging from 33% to 60% included, and a slight variation in the mean absolute differences. There was no significant difference between the FEA results for control constraint level and for 33% constraint. However, fluctuations occurred in more proximal levels of constraint, with a critical mean absolute difference (SvM condition) for 67% integration of total tibia length, and higher values for the most proximal level of 75%. Lastly, for all variables, the mean absolute differences between integration levels 33% and 75% were doubled for both the OSS and SED conditions, and tripled for the SvM. Relatively small variation in the slope coefficient (a) and the coefficient of determination (R^2) were observed for the 75% level. Concerning the

Table 5. Mean \pm SD of the parameters used to compare the FEA results within the VOI to the result for the 5% fully constrained level. Mean and standard deviation are calculated from the results obtained for each of the 9 subjects. A slope (a) of 1 and a coefficient of determination of 1 indicate results very close to that of the 5% fully constrained level. Global absolute difference is the absolute difference between the current model output fields and the output fields for the 5% constrained model, the values were then normalized by the median value of the model constrained at 5% of the tibia length.

Comp. 5% vs	Octohedral Shear Strain (OSS)				Strain Energy Density (SED)				von Mises equivalent Stress (SvM)							
	Linear regression parameters		Global absolute differences (%)		Linear regression parameters		Global absolute differences (%)		Linear regression parameters		Global absolute differences (%)					
	a (slope)	R ²	Global absolute differences (%)	Global absolute differences (%)	a (slope)	R ²	Global absolute differences (%)	Global absolute differences (%)	a (slope)	R ²	Global absolute differences (%)	Global absolute differences (%)				
CTL_TO	33%	1,0000 \pm 0,0000	1,0000 \pm 0,0000	0,0000	\pm	0,0000	1,0000 \pm 0,0000	1,0000 \pm 0,0000	0,0000	\pm	0,0000	1,0000 \pm 0,0000	1,0000 \pm 0,0000	0,0000	\pm	0,0000
	50%	1,0000 \pm 0,0000	1,0000 \pm 0,0000	0,0002	\pm	0,0002	1,0000 \pm 0,0000	1,0000 \pm 0,0000	0,0014	\pm	0,0012	1,0000 \pm 0,0000	1,0000 \pm 0,0000	0,0004	\pm	0,0004
	60%	1,0000 \pm 0,0000	1,0000 \pm 0,0000	0,0054	\pm	0,0048	1,0001 \pm 0,0001	1,0000 \pm 0,0000	0,0537	\pm	0,0691	1,0000 \pm 0,0000	1,0000 \pm 0,0000	0,0156	\pm	0,0173
	67%	0,9997 \pm 0,0002	1,0000 \pm 0,0000	0,0687	\pm	0,0461	0,9997 \pm 0,0004	1,0000 \pm 0,0000	0,3931	\pm	0,2114	0,9999 \pm 0,0001	1,0000 \pm 0,0000	0,1284	\pm	0,0692
75%	0,9954 \pm 0,0026	0,9987 \pm 0,0007	0,8750	\pm	0,4416	0,9837 \pm 0,0069	0,9986 \pm 0,0008	7,1714	\pm	2,8139	0,9933 \pm 0,0022	0,9993 \pm 0,0004	2,1293	\pm	0,9283	
CTL_HS	33%	1,0000 \pm 0,0000	1,0000 \pm 0,0000	0,0000	\pm	0,0000	1,0000 \pm 0,0000	1,0000 \pm 0,0000	0,0000	\pm	0,0000	1,0000 \pm 0,0000	1,0000 \pm 0,0000	0,0000	\pm	0,0000
	50%	1,0000 \pm 0,0000	1,0000 \pm 0,0000	0,0003	\pm	0,0004	1,0000 \pm 0,0000	1,0000 \pm 0,0000	0,0022	\pm	0,0023	1,0000 \pm 0,0000	1,0000 \pm 0,0000	0,0007	\pm	0,0008
	60%	1,0000 \pm 0,0000	1,0000 \pm 0,0000	0,0093	\pm	0,0067	1,0002 \pm 0,0001	1,0000 \pm 0,0000	0,1036	\pm	0,0822	1,0000 \pm 0,0000	1,0000 \pm 0,0000	0,0302	\pm	0,0216
	67%	0,9998 \pm 0,0002	1,0000 \pm 0,0000	0,0915	\pm	0,0534	0,9999 \pm 0,0003	1,0000 \pm 0,0000	0,4881	\pm	0,2409	0,9999 \pm 0,0001	1,0000 \pm 0,0000	0,1627	\pm	0,0795
75%	0,9963 \pm 0,0028	0,9978 \pm 0,0010	1,0137	\pm	0,4714	0,9806 \pm 0,0080	0,9983 \pm 0,0010	8,2150	\pm	3,0931	0,9917 \pm 0,0022	0,9991 \pm 0,0005	2,5430	\pm	1,0913	
CU	33%	1,0000 \pm 0,0000	1,0000 \pm 0,0000	0,0000	\pm	0,0000	1,0000 \pm 0,0000	1,0000 \pm 0,0000	0,0000	\pm	0,0000	1,0000 \pm 0,0000	1,0000 \pm 0,0000	0,0000	\pm	0,0000
	50%	1,0000 \pm 0,0000	1,0000 \pm 0,0000	0,0003	\pm	0,0003	1,0000 \pm 0,0000	1,0000 \pm 0,0000	0,0042	\pm	0,0036	1,0000 \pm 0,0000	1,0000 \pm 0,0000	0,0010	\pm	0,0008
	60%	1,0000 \pm 0,0000	1,0000 \pm 0,0000	0,0082	\pm	0,0064	1,0000 \pm 0,0000	1,0000 \pm 0,0000	0,1022	\pm	0,0720	1,0000 \pm 0,0000	1,0000 \pm 0,0000	0,0287	\pm	0,0210
	67%	1,0000 \pm 0,0001	1,0000 \pm 0,0000	0,0462	\pm	0,0369	0,9999 \pm 0,0002	1,0000 \pm 0,0000	0,5543	\pm	0,3666	1,0000 \pm 0,0001	1,0000 \pm 0,0000	0,1499	\pm	0,0949
75%	0,9985 \pm 0,0014	0,9982 \pm 0,0012	0,8380	\pm	0,6103	0,9957 \pm 0,0026	0,9987 \pm 0,0010	9,5951	\pm	5,9739	0,9939 \pm 0,0026	0,9991 \pm 0,0007	2,7918	\pm	1,7215	

values of the mean and the standard deviation, there is a noticeable difference between conditions, ranging from control to 60% and conditions higher than 67%.

Discussion

The above results point to substantial differences among FEA results when this PSFEM methodology is applied. They highlight a significant correlation between two choices of material properties in the tibia PSFEM: the nDHeM and DHeM conditions. Heterogeneous and homogenous modelling of the bone material properties yield to important differences in the studied output mechanical fields. This suggests that models not accounting for the heterogeneous distribution of density within the bone could be highly biased. Thus, creating models from only the surface geometry of the bone as those obtained from statistical shape model or pseudo-3D imaging (e.g., EOS) should not be recommended.

This study also confirms that PSFEMs are sensitive to the level of constraint, with FEA results variation depending on the investigated mechanical field (OSS, SED, SvM). Variations between the control level of constraint (5% of total tibia length) and levels of 67% or higher were observed for all subjects concerned. The more proximal the level of constraint, the higher the variation. The constraint level has an impact on the mechanical behaviour of PSFEM in the VOI (20% of the proximal tibia). Consequently, our results suggest that placing the fully constrained distal end of the tibia in PSFEMs at up to 60% of the total tibia length will ensure consistent results in a VOI comprising the proximal 20% of the tibia. To prepare for virtual surgery involving similar VOIs, the CT scan acquisition window needs to include 40% of the proximal tibia to be relevant to PSFEMs. Reducing acquisition window size will benefit both patient (reduced exposure to radiation) and hospital (reduction in resource use) and will facilitate preoperative modelling (easier segmentation and faster finite element simulations).

In our PSFEM of the tibia, we consider the active muscles pulling on the tibia joint without accounting for ligaments. The ligaments passive support function during the simulated activities were assumed negligible relative to muscle and contact forces. Although our study addresses the increase and standardization of criteria to be chosen for the virtual operating theater during the preoperative phase of TKA, we did not apply finite element models to TKA to test our conclusions on clinical cases. It would be very

valuable to extend this work by elaborating finite element models according to the recommendations of this study and then testing them in dynamic conditions. Ex-vivo experimentation on anatomical parts will be essential to validate the presented PSFEM method. However, since this method is based on data from published studies, and the results are comparative, our conclusions should hold even under moderate alteration of the method.

This study highlights the need to reach a scientific consensus on material properties and boundary conditions in PSFEM, to make inter-study comparison feasible and rule out biases.

Acknowledgements

The authors would like to thank Rémy Casanova for his help in processing the data with R, Julien Dupeyroux for his help in writing the manuscript and Marjorie Sweetko for English language revision.

Disclosure statement

The authors have no competing interest to declare.

References

- Adouni M, Shirazi-Adl A, Shirazi R. 2012. Computational biodynamics of human knee joint in gait: from muscle forces to cartilage stresses. *J Biomech.* 45(12):2149–2156. <https://linkinghub.elsevier.com/retrieve/pii/S0021929012003211>.
- Arden N, Nevitt MC. 2006. Osteoarthritis: epidemiology. *Best Pract Res Clin Rheumatol.* 20(1):3–25. <https://linkinghub.elsevier.com/retrieve/pii/S1521694205001087>.
- Au AG, Liggins AB, Raso VJ, Amirfazli A. 2005. A parametric analysis of fixation post shape in tibial knee prostheses. *Med Eng Phys.* 27(2):123–134. <http://www.sciencedirect.com/science/article/pii/S135045330400181X>.
- Baliga BR, Pai BR, Shenoy S, Hegde KA, Rao KS, Swaroop S, Shetkar A. 2018. Effect of posterior tibial slope and implant material on the bone-implant system following TKA: A finite element study. Jin Z, editor. *Cogent Eng.* 5(1):1513771. <https://www.cogentoa.com/article/10.1080/23311916.2018.1513771>.
- Bourne RB, Chesworth BM, Davis AM, Mahomed NN, Charron KDJ. 2010. Patient satisfaction after total knee arthroplasty: Who is satisfied and who is not?. *Clin Orthop Relat Res.* 468(1):57–63.
- Bozic KJ, Kurtz SM, Lau E, Ong K, Chiu V, Vail TP, Rubash HE, Berry DJ. 2010. The epidemiology of revision total knee arthroplasty in the United States. *Clin Orthop Relat Res.* 468(1):45–51. <http://link.springer.com/10.1007/s11999-009-0945-0>.
- Brenner DJ, Hall EJ. 2007. Computed tomography—an increasing source of radiation exposure. *N Engl J Med.* 357(22):2277–2284. <http://www.nejm.org/doi/abs/10.1056/NEJMra072149>.

- Brihault J, Navacchia A, Pianigiani S, Labey L, De Corte R, Pascale V, Innocenti B. 2016. All-polyethylene tibial components generate higher stress and micromotions than metal-backed tibial components in total knee arthroplasty. *Knee Surg Sports Traumatol Arthrosc.* 24(8):2550–2559. <http://link.springer.com/10.1007/s00167-015-3630-8>.
- Castro APG, Completo A, Simões JA, Flores P. 2015. Biomechanical behaviour of cancellous bone on patellofemoral arthroplasty with Journey prosthesis: a finite element study. *Comput Methods Biomech Biomed Eng.* 18(10):1090–1098. <http://www.tandfonline.com/doi/abs/10.1080/10255842.2013.870999>.
- Completo A, Talaia P, Fonseca F, Simões JA. 2009. Relationship of design features of stemmed tibial knee prosthesis with stress shielding and end-of-stem pain. *Mater Des.* 30(4):1391–1397. <http://dx.doi.org/10.1016/j.matdes.2008.06.071>.
- DeFrate LE, Nha KW, Papannagari R, Moses JM, Gill TJ, Li G. 2007. The biomechanical function of the patellar tendon during in-vivo weight-bearing flexion. *J Biomech.* 40(8):1716–1722. <https://linkinghub.elsevier.com/retrieve/pii/S0021929006003216>.
- van Eijnatten M, van Dijk R, Dobbe J, Streekstra G, Koivisto J, Wolff J. 2018. CT image segmentation methods for bone used in medical additive manufacturing. *Med Eng Phys.* 51:6–16. <https://linkinghub.elsevier.com/retrieve/pii/S1350453317302631>.
- El-Zayat BF, Heyse TJ, Fanciullacci N, Labey L, Fuchs-Winkelmann S, Innocenti B. 2016. Fixation techniques and stem dimensions in hinged total knee arthroplasty: a finite element study. *Arch Orthop Trauma Surg.* 136(12):1741–1752. <http://link.springer.com/10.1007/s00402-016-2571-0>.
- Guillemin F, Rat AC, Mazieres B, Pouchot J, Fautrel B, Euller-Ziegler L, Fardellone P, Morvan J, Roux CH, Verrouil E, et al. 2011. Prevalence of symptomatic hip and knee osteoarthritis: A two-phase population-based survey. *Osteoarthr Cartil.* 19(11):1314–1322.
- He Y, Burkhalter D, Durocher D, Gilbert JM. 2018. Solid-lattice hip prosthesis design: applying topology and lattice optimization to reduce stress shielding from hip implants. In: 2018 Design of Medical Devices Conference. Minneapolis, Minnesota: ASME. p. V001T03A001. <http://proceedings.asmedigitalcollection.asme.org/proceeding.aspx?doi=10.1115/DMD2018-6804>.
- Helgason B, Perilli E, Schileo E, Taddei F, Brynjólfsson S, Viceconti M. 2008. Mathematical relationships between bone density and mechanical properties: A literature review. *Clin Biomech.* 23(2):135–146. <http://www.sciencedirect.com/science/article/pii/S0268003307001866>.
- Heyland M, Trepczynski A, Duda GN, Zehn M, Schaser KD, Märdian S. 2015. Selecting boundary conditions in physiological strain analysis of the femur: Balanced loads, inertia relief method and follower load. *Med Eng Phys.* 37(12):1180–1185.
- Innocenti B, Pianigiani S, Ramundo G, Thienpont E. 2016. Biomechanical effects of different varus and valgus alignments in medial unicompartmental knee arthroplasty. *J Arthroplasty.* 31(12):2685–2691. <https://linkinghub.elsevier.com/retrieve/pii/S0883540316303618>.
- Keaveny TM, Hayes WC. 1993. A 20-year perspective on the mechanical properties of trabecular bone. *J Biomech.* 115(4B):534–542. <http://biomechanical.asmedigitalcollection.asme.org/article.aspx?articleid=1399632>.
- Kistler M, Bonaretti S, Pfaher M, Niklaus R, Buehler P. 2013. The virtual skeleton database: an open access repository for biomedical research and collaboration. *J Med Internet Res.* 15(11):e245.
- Knowles NK, Reeves JM, Ferreira LM. 2016. Quantitative Computed Tomography (QCT) derived Bone Mineral Density (BMD) in finite element studies: a review of the literature. *J Exp Orthop.* 3(1):36. <http://jeo-esska.springeropen.com/articles/10.1186/s40634-016-0072-2>.
- Kuster MS, Wood GA, Stachowiak GW, Gächter A. 1997. Joint load considerations in total knee replacement. *J Bone Jt Surg - Ser B.* 79-B(1):109–113.
- Maradit Kremers H, Larson DR, Crowson CS, Kremers WK, Washington RE, Steiner CA, Jiranek WA, Berry DJ. 2015. Prevalence of total hip and knee replacement in the United States. *J Bone Jt Surgery-American.* 97(17):1386–1397. <https://insights.ovid.com/crossref?an=00004623-201509020-00002>.
- Mesfar W, Shirazi-Adl A. 2006. Knee joint mechanics under quadriceps-hamstrings muscle forces are influenced by tibial restraint. *Clin Biomech.* 21(8):841–848. <https://linkinghub.elsevier.com/retrieve/pii/S0268003306000854>.
- Munier M, Donnez M, Ollivier M, Flecher X, Chabrand P, Argenson J-N, Parratte S. 2017. Can three-dimensional patient-specific cutting guides be used to achieve optimal correction for high tibial osteotomy? Pilot study. *Orthop Traumatol Surg Res.* 103(2):245–250. <https://linkinghub.elsevier.com/retrieve/pii/S1877056817300294>.
- Polgár K, Viceconti M, O'Connor JJ. 2001. A comparison between automatically generated linear and parabolic tetrahedra when used to mesh a human femur. *Proc Inst Mech Eng H.* 215(1):85–94. <http://www.ncbi.nlm.nih.gov/pubmed/11323989>.
- Rho JY, Hobatho MC, Ashman RB. 1995. Relations of mechanical properties to density and CT numbers in human bone. *Med Eng Phys.* 17(5):347–355.
- Sasaki K, Neptune RR. 2010. Individual muscle contributions to the axial knee joint contact force during normal walking. *J Biomech.* 43(14):2780–2784. <http://dx.doi.org/10.1016/j.jbiomech.2010.06.011>.
- Stadelmann VA, Hocké J, Verhelle J, Forster V, Merlini F, Terrier A, Pioletti DP. 2009. 3D strain map of axially loaded mouse tibia: a numerical analysis validated by experimental measurements. *Comput Methods Biomech Biomed Engin.* 12(1):95–100.
- Taddei F, Cristofolini L, Martelli S, Gill HS, Viceconti M. 2006a. Subject-specific finite element models of long bones: An in vitro evaluation of the overall accuracy. *J Biomech.* 39(13):2457–2467. <http://www.sciencedirect.com/science/article/pii/S0021929005003568>.
- Taddei F, Martelli S, Reggiani B, Cristofolini L, Viceconti M. 2006b. Finite-element modeling of bones from CT data: sensitivity to geometry and material uncertainties. *IEEE Trans Biomed Eng.* 53(11):2194–2200. <http://ieeexplore.ieee.org/document/1710160/>.
- Taddei F, Schileo E, Helgason B, Cristofolini L, Viceconti M. 2007. The material mapping strategy influences the accuracy of CT-based finite element models of bones: an evaluation against experimental measurements. *Med Eng Phys.* 29(9):973–979.

- Taylor M, Prendergast PJ. 2015. Four decades of finite element analysis of orthopaedic devices: where are we now and what are the opportunities? *J Biomech.* 48(5): 767–778. <http://www.sciencedirect.com/science/article/pii/S0021929014006733>.
- Taylor WR, Heller MO, Bergmann G, Duda GN. 2004. Tibio-femoral loading during human gait and stair climbing. *J Orthop Res.* 22(3):625–632. <http://doi.wiley.com/10.1016/j.orthres.2003.09.003>.
- Thompson SM, Yohuno D, Bradley WN, Crocombe AD. 2016. Finite element analysis: a comparison of an all-polyethylene tibial implant and its metal-backed equivalent. *Knee Surgery, Sport Traumatol Arthrosc.* 24(8):2560–2566. <http://link.springer.com/10.1007/s00167-015-3923-y>.
- Viceconti M, Bellingeri L, Cristofolini L, Toni A. 1998. A comparative study on different methods of automatic mesh generation of human femurs. *Med Eng Phys.* 20(1):1–10. <https://linkinghub.elsevier.com/retrieve/pii/S1350453397000490>.
- Williams JL, Lewis JL. 1982. Properties and an anisotropic model of cancellous bone from the proximal tibial epiphysis. *J Biomech Eng.* 104(1):50–56. <http://biomechanical.asmedigitalcollection.asme.org/article.aspx?articleid=1395556>.
- Winby CR, Lloyd DG, Besier TF, Kirk TB. 2009. Muscle and external load contribution to knee joint contact loads during normal gait. *J Biomech.* 42(14):2294–2300. <http://dx.doi.org/10.1016/j.jbiomech.2009.06.019>.
- Wolff J. 1893. Das gesetz der transformation der knochen. *Dtsch Med Wochenschr.* 19(47):1222–1224. <http://www.thieme-connect.de/DOI/DOI?>